

On the Interstellar Extinction Curve toward HD 93222, A Sightline with an Exceedingly Narrow 2175 Å Extinction Bump

Qian Wang^{1,2}, Aigen Li², and X.J. Yang^{1,2}

ABSTRACT

The 2175 Å extinction bump, the most prominent spectral feature superimposed on the interstellar extinction curve, is widely seen in the interstellar medium (ISM) of the Milky Way and external galaxies, both near and far. While its central wavelength is remarkably stable and independent with environment, its width shows considerable variation and environmental dependence. Here we examine the extinction curve for the line of sight toward HD 93222, a young star located in the Carina nebula. It is found that the 2175 Å bump is extremely sharp, which is among the narrowest ever found in the Milky Way and external galaxies. We model the derived extinction curve and find that, to explain the extinction characteristics of HD 93222, in addition to the conventional silicate and graphite dust mixture, an additional population of nano-sized graphitic grains is required.

Subject headings: dust, extinction — ISM: lines and bands — ISM: molecules

1. INTRODUCTION

First detected six decades ago by Stecher (1965), the 2175 Å extinction bump, spanning roughly the wavelength range between 1700 and 2700 Å, is the most prominent spectral feature superimposed on the interstellar extinction curve. It is now widely seen in the Milky Way and nearby galaxies including M31, the Large Magellanic Cloud, and several regions in the Small Magellanic Cloud (e.g., see Fitzpatrick 1986, Bianchi et al. 1996, Gordon & Clayton 1998, Misselt et al. 1999, Clayton et al. 2000, Gordon et al. 2003, Valencic et al.

¹Department of Physics, Xiangtan University, 411105 Xiangtan, Hunan Province, China; xjyang@xtu.edu.cn

²Department of Physics and Astronomy, University of Missouri, Columbia, MO 65211, USA lia@missouri.edu

2004, Fitzpatrick & Massa 2007, Maíz-Apellániz & Rubio 2012, Dong et al. 2014, Clayton et al. 2015, Decleir et al. 2019, Wang et al. 2022). It has also been seen in more distant galaxies, including gravitational lens galaxies and damped Ly α absorbers at redshifts $z \lesssim 1$ (e.g., see Motta et al. 2002), dusty intervening MgII systems at $z \lesssim 2$ toward quasars (see Wang et al. 2004; Srianand et al. 2008; Zhou et al. 2010; Jiang et al. 2011; Ma et al. 2015, 2017), star-forming galaxies at $1 < z < 3$ (e.g., see Noll et al. 2007, 2009; Conroy et al. 2010; Kriek et al. 2013; Battisti et al. 2020; Shvarei et al. 2022), and gamma-ray burst host galaxies at various redshifts (Elíasdóttir et al. 2009; Liang & Li 2009, 2010; Prochaska et al. 2009; Zafar et al. 2011, 2012). In the era of the *James Webb Space Telescope* (JWST), the 2175 Å extinction bump has recently also been seen in the cosmic dawn at $z \gtrsim 6$ (see Witstok et al. 2023; Markov et al. 2023, 2025a, 2025b; Ormerod et al. 2025; Fisher et al. 2025).

The most striking characteristics of the 2175 Å extinction bump are the invariant central wavelength and variable bandwidth. Its peak position at 2175 Å ($4.6 \mu\text{m}^{-1}$) is remarkably constant and only varies by $\pm 0.46\%$ (2σ ; see Wang et al. 2023). In contrast, its full width half maximum (FWHM) varies by $\pm 12\%$ (2σ) around 469 Å ($\approx 1 \mu\text{m}^{-1}$; see Fitzpatrick & Massa 1986, Valencic et al. 2004).

In this work, we explore the 2175 Å extinction bump for the line of sight toward HD 93222, a young star located in the Carina nebula, which is among the sharpest ever found in the Milky Way and external galaxies. This paper is structured as follows. We first derive in §2 the extinction curve of HD 93222 from the far ultraviolet (UV) to the near infrared (IR). We model the derived extinction curve in §3 in terms of the standard silicate-graphite interstellar dust model aided by an additional nano carbon dust population. The results are summarized in §4.

2. The Extinction Curve

HD 93222 is a young star of a spectral type of O7 IIIIf, located in the Carina nebula, a large and complex region of bright and dark nebulosity in the constellation Carina. This nebula lies within the Carina-Sagittarius arm of the Milky Way and is one of the largest star-forming regions of the Milky Way, situated $\sim 2,600$ pc from Earth (Markova et al. 2018).

We first determine the UV extinction in the wavelength range of $3.3 < \lambda^{-1} < 8.7 \mu\text{m}^{-1}$ by comparing the dust-obscured spectrum of HD 93222 obtained with the *International Ultraviolet Explorer* (IUE) with the intrinsic, unreddened spectra of stars of the same spectral type as HD 93222. The IUE spectra were taken from the *Mikulski Archive for Space Tele-*

scopes¹, including data from three cameras: the Short-Wavelength Prime (SWP) Camera covering ~ 1150 — 1978 Å, and the two long-wavelength cameras, i.e., the Long-Wavelength Prime (LWP) and the Long-Wavelength Redundant (LWR) covering ~ 1850 — 3347 Å. The dust-free intrinsic stellar spectrum is approximated by the stellar atmospheric model spectrum of Castelli & Kurucz (2004).² These stellar atmosphere models are characterized by four parameters: the stellar effective temperature T_{eff} , gravity $\log g$, metallicity [M/H], and microturbulence ξ . Taking the spectral type to be O7 IIIIf (which determines T_{eff}), we explore a range of stellar model parameters for HD 93222 by varying metallicity and gravity, and select the combination that best fits the observed IUE spectrum. The stellar parameters of HD 93222, including T_{eff} , $\log g$, [M/H], distance (d), luminosity (L_{\star}), and stellar radius (R_{\star}) are listed in Table 1.

The extinction at wavelength λ is denoted by A_{λ} . The observed IUE spectrum (F_{λ}^{obs}) and the intrinsic, dust-free stellar spectrum (F_{λ}^{int}) are related through dust extinction

$$F_{\lambda}^{\text{obs}} = F_{\lambda}^{\text{int}} \exp \left(-\frac{A_{\lambda}}{A_V} \frac{A_V}{1.086} \right). \quad (1)$$

Let F_{ν}^{RK} be the Kurucz model atmospheric flux of Castelli & Kurucz (2004) at stellar surface (in unit of $\text{erg s}^{-1} \text{cm}^{-2} \text{Hz}^{-1}$). At an Earth–stellar distance of d , the dust-free intrinsic flux (in unit of $\text{erg s}^{-1} \text{cm}^{-3}$) would be

$$F_{\lambda}^{\text{int}} = F_{\nu}^{\text{RK}} \times \frac{c}{\lambda^2} \times \left(\frac{R_{\star}}{d} \right)^2, \quad (2)$$

where c is the speed of light.

Following Fitzpatrick & Massa (1988; hereafter FM88), we represent the wavelength-dependence of extinction by an analytical formula consisting of three parts,

$$\frac{A_{\lambda}}{A_V} = c_1 + c_2 x + c_3 D(x; \gamma, x_0) + c_4 F(x), \quad (3)$$

where $x \equiv \lambda^{-1}$ is the inverse wavelength (or wavenumber); $c_1 + c_2 x$ is the linear background; $D(x; \gamma, x_0)$, a Drude function of width γ (in unit of μm^{-1}) peaking at x_0 (also in unit of μm^{-1}) which characterizes the 2175 Å extinction bump, is defined as

$$D(x; \gamma, x_0) = \frac{x^2}{(x^2 - x_0^2)^2 + x^2 \gamma^2}; \quad (4)$$

¹<https://archive.stsci.edu/iue/>

²<http://kurucz.harvard.edu/grids/gridxxxodfnew>

and $F(x)$ is the far-UV nonlinear rise at $x > 5.9 \mu\text{m}^{-1}$ as described by

$$F(x) = \begin{cases} 0.5392(x - 5.9)^2 + 0.05644(x - 5.9)^3 & x \geq 5.9 \mu\text{m}^{-1} , \\ 0 & x < 5.9 \mu\text{m}^{-1} . \end{cases} \quad (5)$$

We make use of the Levenberg–Marquardt algorithm to fit the observed spectrum (see eq. 1) by minimizing χ^2 . The best-fitting parameters x_0 , γ , c_1 , c_2 , c_3 , and c_4 are listed in Table 2. Figure 1 shows the observed IUE spectrum (F_λ^{obs}) in comparison with the Kurucz model-based, extinction-free “intrinsic” spectrum (F_λ^{int}), as well as the best-fitting, dust-obscured Kurucz model spectrum ($F_\lambda^{\text{int}} \exp\{-A_\lambda/1.086\}$). Also shown is the derived extinction curve and its three components, i.e., the linear background, the 2175 Å bump, and the far-UV rise. We note that this approach actually determines $c_j \times A_V$ (where $j = 1, 2, 3, 4$), i.e., c_j and A_V are degenerated. To break this degeneracy, we adopt $A_V = R_V \times E(B - V) \approx 1.71$ mag, where $E(B - V) \approx 0.35$ mag is the reddening (Fitzpatrick et al. 2019) and $R_V \equiv A_V/E(B - V) \approx 4.76$ is the optical total-to-selective extinction ratio (Valencic et al. 2004). We will discuss the choice of R_V in §3.3.

We also need to construct the extinction curve at $\lambda^{-1} < 3.3 \mu\text{m}^{-1}$. To this end, we employ the parametrization of Cardelli, Clayton, & Mathis (1989; hereafter CCM) who found that most of the Galactic interstellar extinction curves can be parametrized by a single parameter R_V . For $1.1 < \lambda^{-1} < 3.3 \mu\text{m}^{-1}$, we derive A_λ/A_V from the CCM parameterization for $R_V = 4.76$. However, a discontinuity often arises between the FM88 parameterization at $\lambda^{-1} > 3.3 \mu\text{m}^{-1}$ and the CCM parameterization at $\lambda^{-1} < 3.3 \mu\text{m}^{-1}$. To ensure a smooth transition and maintain consistency with the observed extinction-to-gas ratio A_V/N_{H} , we apply a scaling factor to the FM88 curve, allowing it to seamlessly match the CCM curve.

For $\lambda^{-1} < 1.1 \mu\text{m}^{-1}$, we approximate the extinction curve by the model extinction calculated from the standard silicate-graphite-PAH model of Weingartner & Draine (2001; WD01) for $R_V = 3.1$, or the extinction calculated by Wang, Li & Jiang (2015; WLJ15). The WLJ15 model is essentially an extension of WD01, but includes an additional population of very large, micron-sized graphite grains which are introduced to account for the observed flat mid-IR extinction at $3 < \lambda < 8 \mu\text{m}$. Figure 2 presents the extinction curve derived for HD 93222, spanning from the far-UV to the near-IR. The black squares indicate the broadband photometric extinction data measured in the U, B, V, J, H, and K bands. It appears that the WLJ15 extinction model is a better choice since it better matches the K band extinction (see Figure 2).

3. Discussion

3.1. The Exceedingly Narrow 2175 Å Extinction Bump of HD 93222

Figure 2 compares the extinction curve derived in §2 for HD 93222 and the CCM representation for $R_V = 4.76$, an optical total-to-selective extinction ratio of HD 93222 (Valencic et al. 2004). It is apparent that, with a FWHM of $\gamma \approx 0.76 \mu\text{m}^{-1}$, the 2175 Å extinction bump of HD 93222 is appreciably narrower and weaker than that of the CCM $R_V = 4.76$ curve. However, the far-UV extinction rise of HD 93222 is considerably steeper than that of the CCM $R_V = 4.76$ curve. As a matter of fact, the far-UV extinction rise of HD 93222 resembles that of the CCM $R_V = 3.1$ curve, which is commonly taken to represent the mean extinction curve of the Galactic diffuse ISM. Indeed, the curvature of the HD 93222 curve at $\lambda^{-1} > 5.9 \mu\text{m}^{-1}$ is essentially the same as that of the CCM $R_V = 3.1$ curve. Figure 2 also shows that the 2175 Å bump is considerably narrower than that of the CCM curves of $R_V = 4.76$ and $R_V = 3.1$.

HD 93222 serves as a striking example of sightlines exhibiting an unusually narrow extinction bump at 2175 Å. The extinction curve of HD 93222 derived in §2 shows a bump centered at $\sim 2190 \text{ \AA}$, which only slightly deviates from the canonical 2175 Å. The most pronounced characteristics of the extinction bump of HD 93222 is its width: with $\gamma \approx 0.76 \mu\text{m}^{-1}$, it is considerably narrower than that of the Galactic diffuse ISM for which the average width is $\sim 0.92 \mu\text{m}$ (Valencic et al. 2004, Fitzpatrick & Massa 2007). To our knowledge, the extinction bump of HD 93222 is one of the narrowest ever observed in the Galactic interstellar lines of sight. Figure 4 illustrates those five sightlines of which the extinction bump is among the narrowest in 328 Galactic interstellar sources (Valencic et al. 2004): HD 164816 ($\gamma \approx 0.78 \mu\text{m}$), HD 172140 ($\gamma \approx 0.77 \mu\text{m}$), NGC 4755 ($\gamma \approx 0.77 \mu\text{m}$), HD 93028 ($\gamma \approx 0.76 \mu\text{m}$), and HD 93222 ($\gamma \approx 0.76 \mu\text{m}$). Figure 4 also compares the bump width γ with R_V^{-1} . It is clear that γ exhibits no obvious relationship with R_V^{-1} , consistent with the earlier finding of Cardelli et al. (1989).

The width of the 2175 Å bump is thought to reflect the size distribution, structural order, and processing history of the bump carrier (and other dust components as well). The unusual characteristics of the extinction bump observed toward HD 93222 may indicate atypical physical conditions along its line of sight, including strong processing by UV starlight from star formation activities, selective fragmentation of grain structures, or a deficiency in large aromatic carbonaceous compounds. This exceptionally narrow bump thus provides a valuable test case for constraining dust models and offers unique insights into the physical nature and origin of the 2175 Å extinction bump.

3.2. Modeling the Extinction Curve

We fit the extinction curve of HD 93222 in terms of the standard silicate–graphite interstellar grain model. For simplicity, we assume the dust to be spherical in shape. We adopt an exponentially-cutoff power-law size distribution for both components: $dn_i/da = n_{\text{H}} B_i a^{-\alpha_i} \exp(-a/a_{c,i})$ for the size range of $50 \text{ \AA} < a < 2.5 \mu\text{m}$, where a is the spherical radius of the dust, n_{H} is the number density of H nuclei, dn_i is the number density of dust of type i with radii in the interval $[a, a+da]$, α_i and $a_{c,i}$ are respectively the power index and exponential cutoff size for dust of type i , and B_i is the constant related to the total amount of dust of type i . The total extinction per H column at wavelength λ is given by

$$A_{\lambda}/N_{\text{H}} = 1.086 \sum_i \int da \frac{1}{n_{\text{H}}} \frac{dn_i}{da} C_{\text{ext},i}(a, \lambda), \quad (6)$$

where the summation is over the two grain types (i.e., amorphous silicate and graphite), and $C_{\text{ext},i}(a, \lambda)$ is the extinction cross section of grain type i of size a at wavelength λ which can be calculated from Mie theory (Bohren & Huffman 1983) using the dielectric functions of “astronomical” silicate and graphite of Draine & Lee (1984).

Figure 5a compares the best-fit model extinction curve with that observationally derived for HD 93222. The best-fit model parameters (i.e., Model #1) are tabulated in Table 3. It is apparent that, although the overall fit is not too bad, the model predicts an extinction bump appreciably too broad to agree with the observed one. Also, the model considerably deviates from the observed one at $1.1 < \lambda^{-1} < 4.2 \mu\text{m}^{-1}$. It is worth noting that the difficulty of fitting the extinction curve of HD 93222 derived by Valencic et al. (2004) has already been recognized by Zuo et al. (2021b).

To reproduce the observed narrow 2175 Å extinction bump, we introduce an additional dust component: a population of nano-sized graphite grains (or “very small grains”, VSG) with a log-normal size distribution, $dn/d\ln a \propto \exp\{-[\ln(a/a_0)]^2/(2\sigma^2)\}$, where a_0 and σ characterize the peak and width of this distribution.³ Let $[\text{C}/\text{H}]_{\text{nano}}$ be the amount of C (relative to H) tied up in the nano graphitic grain component. Figure 5b shows the best-fit model which includes, in addition to amorphous silicate and graphite grains, an extra population of nano graphitic grains of $[\text{C}/\text{H}]_{\text{nano}} = 40 \text{ ppm}$. We take $a_0 = 10 \text{ \AA}$ and $\sigma = 0.4$. The exact choice of a_0 and σ does not matter much as long as this extra component is nano-sized so that the nano-graphitic grains are in the Rayleigh regime (i.e., $2\pi a/\lambda \ll 1$).⁴

³For this distribution, $a^3 dn/d\ln a$ peaks at $a_p = a_0 \exp(3\sigma^2)$.

⁴In the Rayleigh regime, the extinction is dominated by absorption and the absorption cross section (on a per unit volume basis) is independent of grain size.

As shown in Figure 5b, the inclusion of a population of nano graphite grains significantly improves the fit to the observed extinction curve, including the narrow 2175 Å extinction bump. Table 3 also tabulates the corresponding model parameters (see Model #2). We admit that the model extinction curve deviates from the “observed” one at $1.2 < \lambda^{-1} < 3.3 \mu\text{m}^{-1}$. We note that the “observed” extinction curve in this range is not really derived from observations. It was constructed from the R_V -based CCM parameterization (see §2). As the CCM parameterization may not be valid for every individual sightline, we shall not worry too much about the deviation at this range. Finally, we have also explored different choices of $[\text{C}/\text{H}]_{\text{nano}}$. Figure 6 shows the best-fit extinction model curves obtained with $[\text{C}/\text{H}]_{\text{nano}} = 30 \text{ ppm}$ (see Figure 6a) and 50 ppm (see Figure 6b). Apparently, the $[\text{C}/\text{H}]_{\text{nano}} = 30 \text{ ppm}$ model under-predicts the observed 2175 Å extinction bump, while the $[\text{C}/\text{H}]_{\text{nano}} = 50 \text{ ppm}$ model over-predicts the observed bump. The model parameters are also tabulated in Table 3 (see Models #3 and #4).

We note that, in principle, the interstellar extinction curve of HD 93222 could also be modeled in terms of composite dust consisting of vacuum and small silicate and amorphous carbon grains (Mathis 1996), or silicate core-carbon mantle grains (Li & Greenberg 1997, Jones et al. 2013). As these models all attribute the 2175 Å bump to small graphitic grains, we expect the quantities and size distributions of these small graphitic grains to be essentially the same as that derived here. The “astrodust” model of Hensley & Draine (2023) assumes an “astrodust” component which resembles the composite dust of Mathis (1996), combined with an additional population of “astronomical” polycyclic aromatic hydrocarbon (PAH) molecules to account for the 2175 Å bump. As the optical properties of astro-PAHs were “designed” to produce an extinction bump with a fixed width of $1.0 \mu\text{m}^{-1}$ (see Li & Draine 2001), the astrodust+PAH model is not expected to reproduce the narrow bump seen in HD 93222. However, this does not mean that PAHs are not able to explain the HD 93222 extinction bump. Totally in the opposite, it is actually very likely that mixtures of specific PAH molecules of different sizes, structures and charging states are expected to be capable of reproducing the bump detected in HD 93222, as demonstrated by Lin et al. (2023, 2025) for the Galactic diffuse ISM and JADES-GS-z6-0, a distant galaxy at $z \approx 6.71$.

3.3. The Interstellar Environments around HD 93222

As illustrated in Figure 7, a dust thermal emission map of the Carina nebula obtained by the *Infrared Astronomical Satellite* (IRAS) at $100 \mu\text{m}$, HD 93222 is located in the southern part of the base of the Carina nebula, one of the largest star-forming regions in the Milky Way, which hosts numerous bright O-type stars. Walborn et al. (1982) detected a strong Mg II and

CII absorption component at -350 km s^{-1} in the IUE data, suggesting a connection with diffuse X-ray emission and near-UV nebulosity. Compared to the other stars in the region, HD 93222 exhibits more discrete velocity structures in its high-ionization lines, indicating a more turbulent environment and stronger stellar winds. The strong radiation field and intense stellar winds around HD 93222 likely lead to the fragmentation of large dust grains into smaller ones and eventually the production of nano graphite grains and a pronounced, sharp 2175 \AA extinction bump.

Also, the prominent CII feature suggests that the surrounding medium is relatively carbon-rich, facilitating the formation of small-sized carbonaceous dust grains widely believed to be responsible for the 2175 \AA extinction bump. The narrow and intense bump observed toward HD 93222 supports this scenario. Moreover, the steep rise in the far-UV extinction (compared to that predicted from the CCM parametrization with $R_V = 4.76$) is also attributed to the abundance of small grains, which are more efficiently produced under such harsh conditions. These factors together contribute to the unique extinction curve observed along the line of sight to HD 93222.

We have so far adopted $R_V = 4.76$ which was derived by Valencic et al. (2004) from the JHK colors using the empirical relations of Fitzpatrick (1999). Although the R_V value derived from such an approach may be subject to large uncertainty, Fitzpatrick & Massa (2007) analyzed the spectral energy distribution of HD 93222 and derived $R_V \approx 5.05$, close to that of Valencic et al. (2004). In general, the value of R_V depends upon the environment along the line of sight. A direction through low-density ISM usually has a rather low R_V (~ 3.1). Lines of sight penetrating into a dense cloud, such as the Ophiuchus or Taurus molecular clouds, usually show $4 < R_V < 6$. However, it is difficult to estimate R_V quantitatively from the environment of a line of sight. We note that Cygni OB2 No. 12 lies behind a dense cloud of dust but has $R_V \approx 3.1$; also, parts of the Taurus molecular cloud have $R_V \sim 3.0\text{--}3.5$ as well (see Mathis 1990 and references therein). Valencic et al. (2004) also cautioned that R_V should not be assigned a physical meaning. Indeed, a large value of $R_V \approx 4.76$ is more appropriate for molecular clouds, the relatively small reddening of $E(B-V) \approx 0.35 \text{ mag}$ for the HD 93222 line of sight (Fitzpatrick et al. 2019) and negligible molecular content⁵ suggest that the sightline toward HD 93222 likely samples diffuse gas.

⁵With an atomic H column density of $N(\text{HI}) \approx 2.95 \times 10^{21} \text{ cm}^{-2}$ and an H₂ column density of $N(\text{H}_2) \approx 0.059 \times 10^{21} \text{ cm}^{-2}$ (Jenkins 2019), the molecular fraction of the HD 93222 sightline is only $f(\text{H}_2) = 2N(\text{H}_2) / [2N(\text{H}_2) + N(\text{HI})] \approx 3.8\%$. With $E(B-V) = 0.35 \text{ mag}$, the extinction-to-gas ratio for the HD 93222 sightline is $A_V/N_{\text{H}} \approx 5.44 \times 10^{-22} \text{ mag cm}^2 \text{ H}^{-1}$ for $R_V = 4.76$, and $\approx 3.65 \times 10^{-22} \text{ mag cm}^2 \text{ H}^{-1}$ for $R_V = 3.2$, both of which are within the typical interstellar ranges of extinction-to-gas ratios (e.g., see Zuo et al. 2021a).

Alternatively, the actual R_V value for the HD 93222 sightline may be appreciably lower than 4.76. Indeed, the R_V value derived from the near-IR photometry tends to be high (e.g., see Patriarchi et al. 2001), whereas, in sharp contrast, R_V based on direct high quality optical photometry yields $R_V \approx 3.19$ (Neckel et al. 1980, Jensen & Snow 2007). Nevertheless, as shown in eqs. 1–5, R_V is not involved in the FM88 parametrization; i.e., for $\lambda^{-1} > 3.3 \mu\text{m}^{-1}$, the shape of the extinction curve and the profile of the 2175 Å bump are independent of the choice of R_V .

It is interesting to note that, as will be shown below, the HD 93222 extinction curve derived from the traditional “pair method” is actually well represented by the CCM $R_V = 3.2$ parametrization. The “pair method” involves photometric or spectrophotometric observations of two stars of identical spectral types, with one star located behind a dust cloud and another star, (in ideal case) unaffected by interstellar dust, so that there is no obscuration between the observer and the star. Let $F_{\lambda, \text{targ}}$ be the observed flux from the reddened, target star at a distance of d_{targ} , and $F_{\lambda, \text{comp}}$ be the flux from the unreddened, comparison star at a distance of d_{comp} . If both stars are of identical spectral and luminosity types, the extinction A_λ —measured in “magnitudes”—is

$$A_\lambda = 2.5 \log \left\{ \frac{F_{\lambda, \text{comp}}}{F_{\lambda, \text{targ}}} \right\} + 5 \log \left\{ \frac{d_{\text{comp}}}{d_{\text{targ}}} \right\} . \quad (7)$$

In our case, the reddened, target star is HD 93222. We take HD 47839 (also known as 15 Mon or S Mon), a brilliant, massive O-type star located in the constellation Monoceros, as the comparison star. If we know accurately the distances of both the target and comparison stars, we can derive from eq. 7 the extinction curve of HD 93222 at $\lambda^{-1} > 3.3 \mu\text{m}^{-1}$ by comparing the IUE spectrum of HD 93222 with that of HD 47839. In Figure 8 we show $A_\lambda = 2.5 \log \{F_{\lambda, \text{comp}}/F_{\lambda, \text{targ}}\} + \text{const}$, the extinction curve of HD 93222 derived from the “pair method”, with a constant offset (const) to account for the often unknown distance term $5 \log \{d_{\text{comp}}/d_{\text{targ}}\}$. The constant offset (const) is determined by matching A_λ with $A_{\lambda, \text{CCM}}$, the extinction predicted from the R_V -based CCM parametrization for HD 93222, where $A_{\lambda, \text{CCM}} = E(B - V) \times \{a(x) R_V + b(x)\}$, $E(B - V) \approx 0.30 \text{ mag}$ is the *reddening difference* between HD 93222 and HD 47839, and the wavelength-dependent coefficients $a(x)$ and $b(x)$ are given in CCM. As shown in Figure 8, with $R_V = 3.2$, we are able to closely match A_λ and $A_{\lambda, \text{CCM}}$, except the $A_{\lambda, \text{CCM}}$ curve predicts a broader 2175 Å extinction bump. We have also applied the FM88 parameterization to fit the HD 93222 extinction curve derived from the “pair method”. Figure 8 clearly shows that a width of $0.76 \mu\text{m}^{-1}$ as derived earlier (see §2) describes well the “pair-method”-derived 2175 Å bump. Again, this demonstrates that the extreme narrowness of the 2175 Å bump derived for HD 93222 is not affected by R_V . Finally, we compare the extinction curve derived from the “pair method” with that derived based on the Kurucz model spectrum (see §2). As shown in Figure 9, the vertically-

shifted extinction curves derived from these two methods, particularly the derived 2175 Å extinction bumps, closely resemble each other. This demonstrates the robustness of the extreme narrowness of the 2175 Å bump of the HD 93222 sightline.

4. Summary

We have determined the extinction curve along the line of sight toward HD 93222 in the Carina nebula which shows an exceedingly narrow 2175 Å extinction bump. With a width of $\gamma \approx 0.76 \mu\text{m}^{-1}$, the extinction bump of the HD 93222 sightline is among the narrowest ever observed in the Milky Way. The derived extinction curve is modeled in terms of the standard silicate-graphite interstellar grain model. It is found that, to explain the observed extinction characteristics of HD 93222, in addition to the conventional silicate and graphite dust mixture, an extra component of nano-sized graphitic grains is required. We argue that this is likely related to the strong radiation field and intense stellar winds around HD 93222.

We thank the anonymous referee for his/her helpful and stimulating comments and suggestions which considerably improved the quality and presentation of this paper. QW and XJY are supported in part by NSFC 12333005 and 12122302, CMS-CSST-2021-A09, Hebei NSF A2023205036, the Innovative Research Group Project of Natural Science Foundation of Hunan Province of China No. 2024JJ1008, and a Postgraduate Scientific Research Innovation Project of Xiangtan University (No. XDCX2023Y155). This work is based on observations made with the International Ultraviolet Explorer (IUE). The data presented in this article were obtained from the Mikulski Archive for Space Telescopes (MAST) at the Space Telescope Science Institute. The specific observations analyzed can be accessed via <https://doi.org/10.17909/ha4q-2y11>.

REFERENCES

Battisti, A. J., Cunha, E. d., Shvai, I., et al. 2020, *ApJ*, 888, 108

Bianchi, L., Clayton, G. C., Bohlin, R. C., et al. 1996, *ApJ*, 471, 203

Bohren, C. F., & Huffman, D. R. 1983, *Absorption and Scattering of Light by Small Particles* (New York: Wiley)

Cardelli, J. A., Clayton, G. C., & Mathis, J. S. 1989, *ApJ*, 345, 245

Castelli, F., & Kurucz, R. L. 2004, arXiv:0405087

Clayton, G. C., Gordon, K. D., & Wolff, M. J. 2000, *ApJS*, 129, 147

Clayton, G. C., Gordon, K. D., Bianchi, L. C., et al. 2015, *ApJ*, 815, 14

Conroy, C. 2010, *MNRAS*, 404, 247

Decleir, M., De Looze, I., Boquien, M., et al. 2019, *MNRAS*, 486, 743

Dong, H., Li, Z., Wang, Q. D., et al. 2014, *ApJ*, 785, 136

Draine, B. T., & Lee, H. M. 1984, *ApJ*, 285, 89

Elíasdóttir, Á., Fynbo, J. P. U., Hjorth, J., et al. 2009, *ApJ*, 697, 1725

Fisher, R., Bowler, R. A. A., Stefanon, M., et al. 2025, *MNRAS*, 539, 109

Fitzpatrick, E. L. 1986, *AJ*, 92, 1068

Fitzpatrick, E. L., & Massa, D. 1986, *ApJ*, 307, 286

Fitzpatrick, E. L., & Massa, D. 1988, *ApJ*, 328, 734

Fitzpatrick, E. L. 1999, *PASP*, 111, 63

Fitzpatrick, E. L., & Massa, D. 2007, *ApJ*, 663, 320

Fitzpatrick, E. L., Massa, D., Gordon, K. D., et al. 2019, *ApJ*, 886, 108

Gordon, K. D., & Clayton, G. C. 1998, *ApJ*, 500, 816

Gordon, K. D., Clayton, G. C., Misselt, K. A., et al. 2003, *ApJ*, 594, 279

Hensley, B. S., & Draine B, T. 2023, *ApJ*, 948, 55

Jenkins, E. B. 2019, *ApJ*, 872, 55

Jensen, A. G., & Snow, T. P. 2007, *ApJ*, 669, 378

Jiang, P., Ge, J., Zhou, H., et al. 2011, *ApJ*, 732, 110

Jones, A. P., Fanciullo, L., Köhler, M., et al. 2013, *A&A*, 558, A62

Kriek, M., & Conroy, C. 2013, *ApJL*, 775, L16

Liang, S. L., & Li, A. 2009, *ApJ*, 690, L56

Liang, S. L., & Li, A. 2010, *ApJ*, 710, 648

Li, A., & Greenberg, J. M. 1997, A&A, 323, 566

Li, A., & Draine, B.T. 2001, ApJ, 554, 778

Lin, Q., Yang, X. J., & Li, A. 2023, MNRAS, 525, 2380

Lin, Q., Yang, X.J., Li, A., & Witstok, J. 2025, A&A, 694, A84

Ma, J., Caucal, P., Noterdaeme, P., et al. 2015, MNRAS, 454, 1751

Ma, J., Ge, J., Zhao, Y., et al. 2017, MNRAS, 472, 2196

Maíz Apellániz, J., & Rubio, M. 2012, A&A, 541, A54

Markov, V., Gallerani, S., Pallottini, A., et al. 2023, A&A, 679, A12

Markov, V., Gallerani, S., Ferrara, A., et al. 2025, Nature Astronomy, 9, 458

Markov, V., Gallerani, S., Pallottini, A., et al. 2025, A&A, 702, A33

Markova, N., Puls, J., & Langer, N. 2018, A&A, 613, A12

Mathis, J. S. 1990, ARA&A, 28, 37

Mathis, J. S. 1996, ApJ, 472, 643

Misselt, K. A., Clayton, G. C., & Gordon, K. D. 1999, 515, 128

Motta, V., Mediavilla, E., Munoz, J. A., et al. 2002, ApJ, 574, 719

Noll, S., Pierini, D., Pannella, M., et al. 2007, A&A, 472, 455

Noll, S., Pierini, D., Cimatti, A., et al. 2009, A&A, 499, 69

Neckel, T., Klare, G., & Sarcander, M. 1980, Bull. Cent. Donnees Stellaires, 19, 61

Ormerod, K., Witstok, J., Smit, R., et al. 2025, MNRAS, 542, 1136

Patriarchi, P., Morbidelli, L., Perinotto, M., et al. 2001, A&A, 372, 644

Prochaska, J. X., Sheffer, Y., Perley, D. A., et al. 2009, ApJ, 691, L27

Shivaei, I., Boogaard, L., Díaz-Santos, T., et al. 2022, MNRAS, 514, 1886

Srianand, R., Gupta, N., Petitjean, P., et al. 2008, MNRAS, 391, L69

Stecher, T. P. 1965, ApJ, 142, 1683

Valencic, L. A., Clayton, G. C., & Gordon, K. D. 2004, *ApJ*, 616, 912

Walborn, N. R., & Hesser, J. E. 1982, *ApJ*, 252, 156

Wang, J., Hall, P. B., Ge, J., et al. 2004, *ApJ*, 609, 589

Wang, Q., Yang, X. J., & Li, A. 2023, *MNRAS*, 525, 983

Wang, S., Li, A., & Jiang, B. W. 2015, *ApJ*, 811, 38

Wang, Y., Gao, J., & Ren, Y. 2022, *ApJS*, 259, 12

Weingartner, J. C., & Draine, B. T. 2001, *ApJ*, 548, 296

Witstok, J., Shivaei, I., Smit, R., et al. 2023, *Nature*, 621, 267

Zafar, T., Watson, D., Fynbo, J. P. U., et al. 2011, *A&A*, 532, A143

Zafar, T., Watson, D., Elíasdóttir, Á., et al. 2012, *ApJ*, 753, 82

Zhou, H., Ge, J., Lu, H., et al. 2010, *ApJ*, 708, 742

Zuo, W.B., Li, A., & Zhao, G. 2021a, *ApJS*, 252, 22

Zuo, W.B., Li, A., & Zhao, G. 2021b, *ApJS*, 257, 63

Table 1: Stellar Parameters of HD 93222

Spectral Type	O7 IIIIf	Fitzpatrick et al. (2019)
$E(B - V)$ (mag)	0.35	Fitzpatrick et al. (2019)
A_V (mag)	1.71	Fitzpatrick et al. (2019)
T_{eff} (K)	38,000	Markova et al. (2018)
$\log g$ (cm s^{-2})	3.9	Markova et al. (2018)
[M/H]	-0.24	Fitzpatrick et al. (2019)
Distance (pc)	2,600	Markova et al. (2018)
$\log(L_{\star}/L_{\odot})$	5.36	Markova et al. (2018)
R_{\star}/R_{\odot}	11	Markova et al. (2018)

Table 2: Extinction Parameters for HD 93222

x_0 (μm^{-1})	4.57 ± 0.01
x_0 (\AA)	2190 ± 0.01
γ (μm^{-1})	0.76 ± 0.01
c_1	0.61 ± 0.01
c_2	0.13 ± 0.00
c_3	0.31 ± 0.00
c_4	0.12 ± 0.01
χ^2	3.00

Table 3: Model Parameters for Fitting the HD 93222 Extinction Curve (with Model #2 Preferred)

Parameters	Model #1	Model #2	Model #3	Model #4
A_V/N_H (10^{-22} mag cm 2 H $^{-1}$)	5.53	5.53	5.53	5.53
Silicate: α_S	3.10	3.20	3.20	3.40
Silicate: $a_{c,S}$ (μm)	0.23	0.24	0.29	0.32
Graphite: α_C	3.10	0.40	0.08	0.20
Graphite: $a_{c,C}$ (μm)	0.24	0.05	0.04	0.05
χ^2/dof	0.098	0.064	0.075	0.12
$[\text{C}/\text{H}]_{\text{nano}}$ (ppm)	0	40	30	50
$[\text{C}/\text{H}]_{\text{dust}}$ (ppm)	220	200	180	220
$[\text{Si}/\text{H}]_{\text{dust}}$ (ppm)	42	35	42	31.5

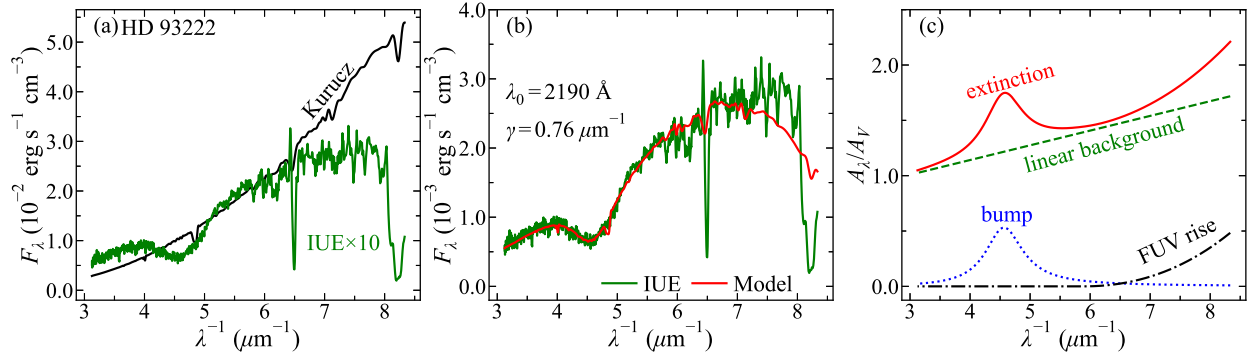


Figure 1: Left panel (a): Comparison of the observed, dust-obscured IUE spectrum (F_λ^{obs} ; green solid line) of HD 93222 with the “intrinsic”, extinction-free spectrum represented by the Kurucz atmospheric model (F_λ^{int} ; black solid line). Note that, to facilitate comparison, the IUE spectrum is multiplied by a factor of 10. Middle panel (b): Comparison of the observed, dust-obscured IUE spectrum (F_λ^{obs} ; green solid line) with the best-fit model spectrum ($F_\lambda^{\text{int}} \exp\{-A_\lambda/1.086\}$; red solid line). Right panel (c): The derived extinction curve expressed as A_λ/A_V for the line of sight toward HD 93222. The red line is the FM88 parametrization at $\lambda^{-1} > 3.3 \mu\text{m}^{-1}$, which is the sum of a linear “background” (green line), a Drude bump of width γ and central position of $x_0 \equiv \lambda_0^{-1}$ (blue line), and a nonlinear far-UV rise (black dash-dotted line) at $\lambda^{-1} > 5.9 \mu\text{m}^{-1}$.

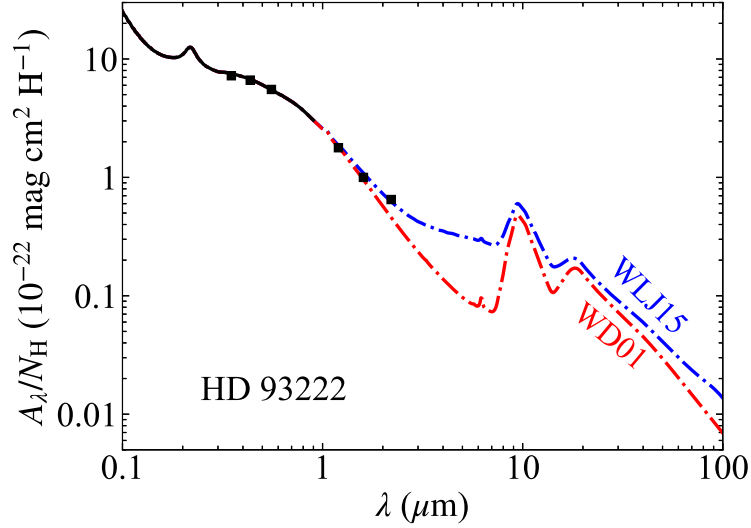


Figure 2: The interstellar extinction curve from the far-UV to the far-IR for the line of sight toward HD 93222, with the FM88 parameterization for $\lambda^{-1} > 3.3 \mu\text{m}^{-1}$, the CCM parameterization (with $R_V = 4.76$) for $1.1 \mu\text{m}^{-1} < \lambda^{-1} < 3.3 \mu\text{m}^{-1}$, and the $R_V = 3.1$ model curves of Weingartner & Draine (2001; red dashed line) and Wang, Li & Jiang (2015; blue dot-dashed line) for $\lambda > 0.9 \mu\text{m}$. The U, B, V, J, H, K photometric extinction data points are superimposed on the extinction curve as black squares.

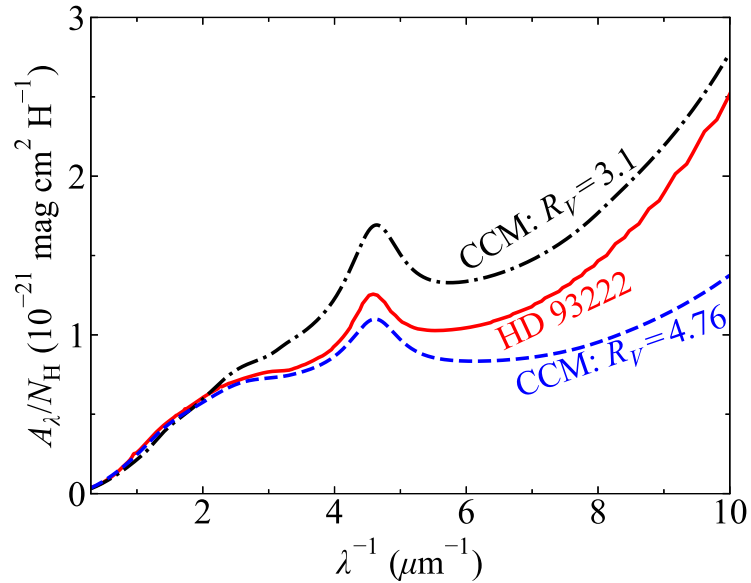


Figure 3: Comparison of the extinction curve derived in §2 for HD 93222 (red solid line) and the CCM representation for $R_V = 4.76$ (blue dashed line), the optical total-to-selective extinction ratio of HD 93222. Also shown is the CCM $R_V = 3.1$ curve (black dot-dashed line), which is commonly taken to represent the mean extinction curve of the Galactic diffuse ISM.

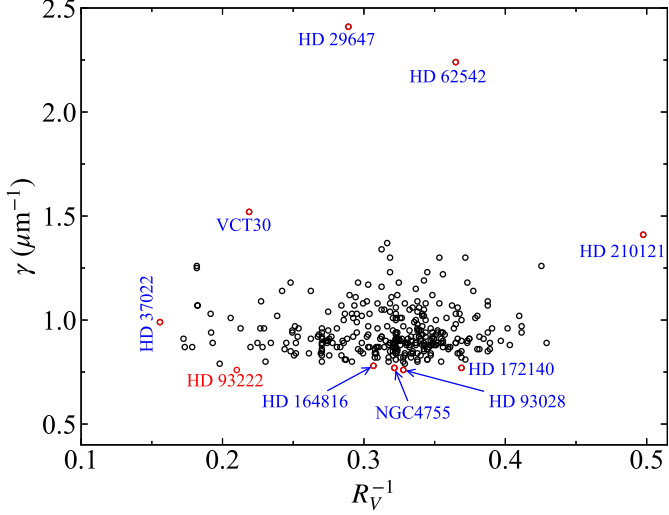


Figure 4: The 2175 Å extinction bump width (FWHM; γ) plotted against R_V^{-1} for the 328 Galactic interstellar extinction curves of Valencic et al. (2004) and Fitzpatrick & Massa (2007). The labelled sightlines (red circles) show those exhibiting extreme γ and R_V values.

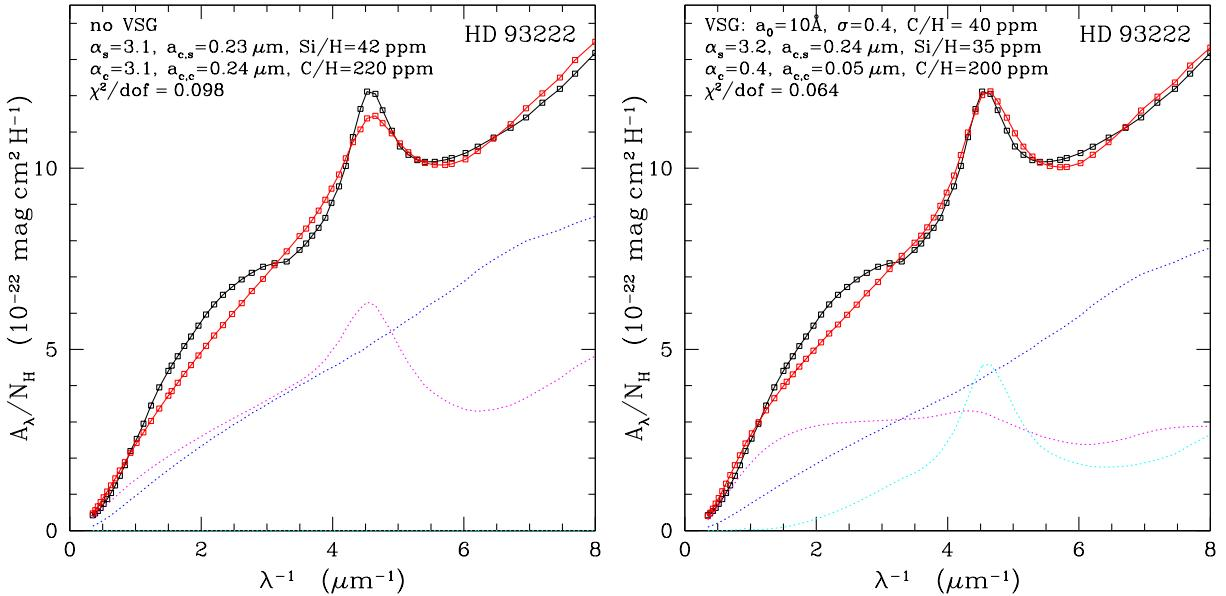


Figure 5: Left panel (a): Fitting the extinction curve of HD 93222 (black squares) with a mixture of silicate (blue dashed line) and graphite grains (magenta dashed line), each with an exponentially-cutoff power-law size distribution (red squares). Right panel (b): Same as (a) but with an additional population of nano graphite grains (cyan dashed line) which lock up a carbon abundance (relative to H) of $[C/H]_{\text{nano}} = 40$ ppm. “VSG” refers to very small grains (i.e., nano graphite grains). The right panel represents our preferred model.

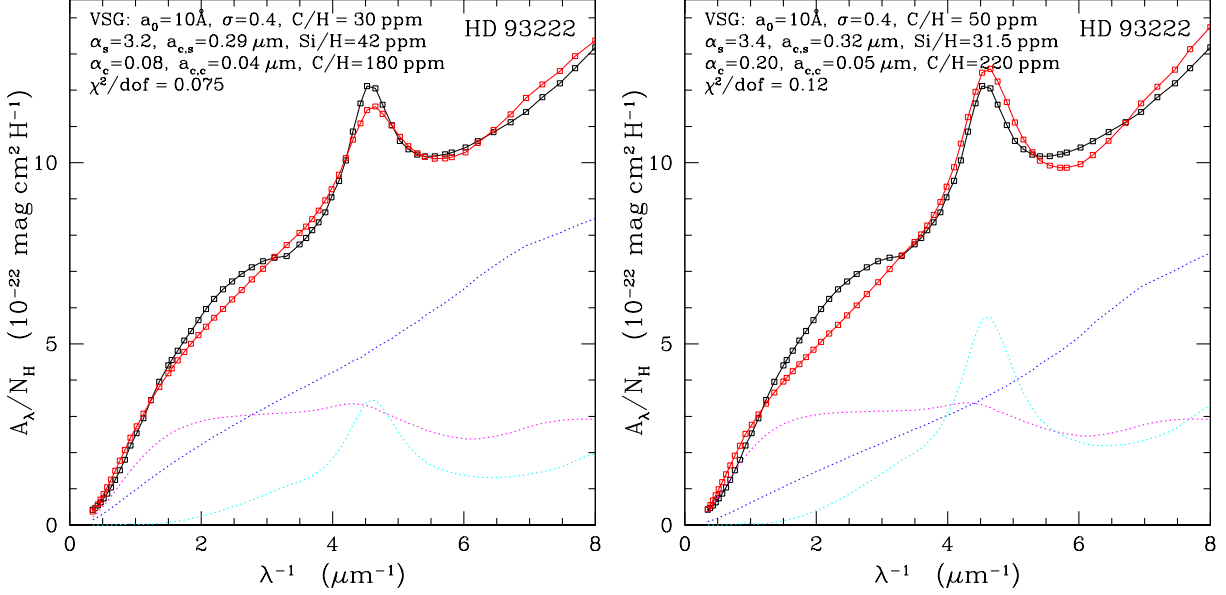


Figure 6: Left panel (a): Same as Figure 5b but with $[C/H]_{\text{nano}} = 30 \text{ ppm}$. Right panel (b): Same as Figure 5b but with $[C/H]_{\text{nano}} = 50 \text{ ppm}$.

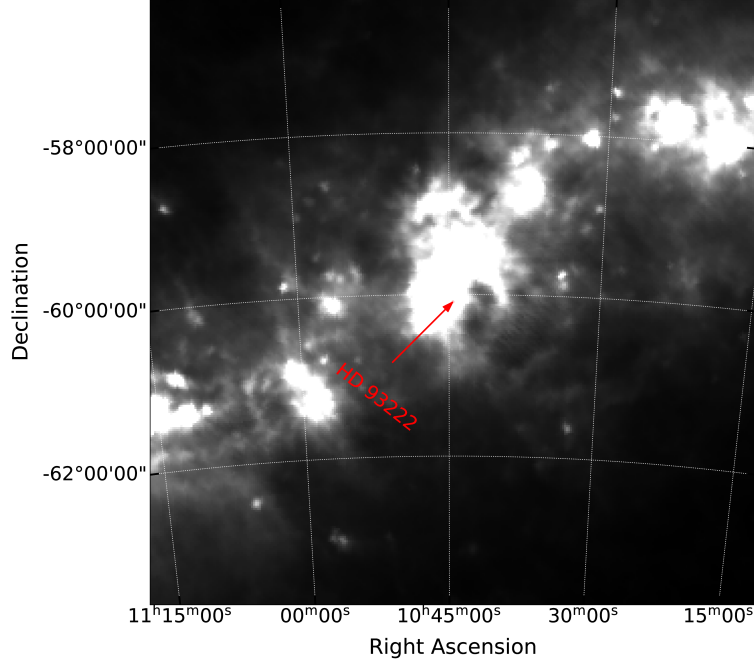


Figure 7: IRAS 100 μm map of the Carina nebula. The position of HD 93222 is also shown.

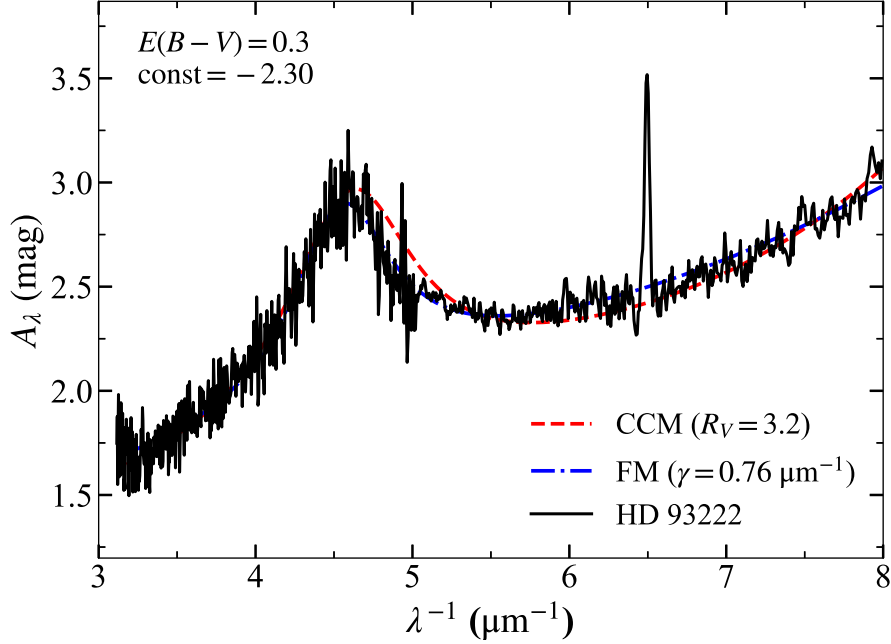


Figure 8: The extinction curve derived from the traditional “pair method” (solid black line) by comparing the IUE spectrum of HD 93222 with that of the comparison star HD 47839, which differ in $E(B - V)$ by ~ 0.3 mag (see §3.3). Also shown are the CCM $R_V = 3.2$ curve (red dashed line) and the FM88 curve (blue dot-dashed line). With a vertical shift of $\text{const} = -2.30$ (see eq. 7), the extinction curve derived from the “pair method” matches the CCM $R_V = 3.2$ curve very well (except the latter has a broader 2175 Å bump). In contrast, the FM88 curve with a narrow bump of $\gamma = 0.76 \mu\text{m}^{-1}$ closely fits the “pair-method”-derived extinction curve.

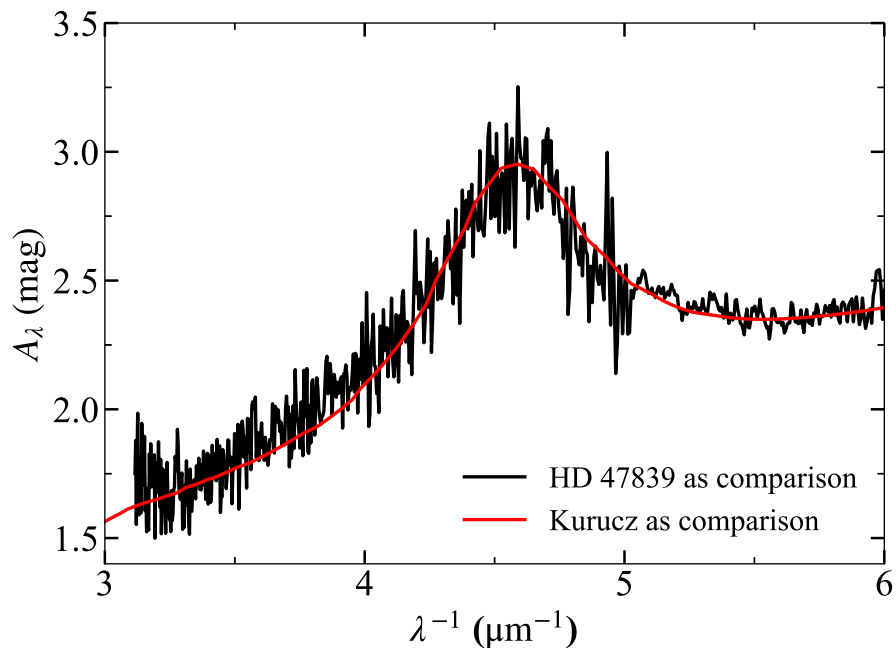


Figure 9: Comparison of the extinction curve derived from the “pair method” (solid black line; see §3.3) with that derived based on the Kurucz model spectrum (solid red line; see §2), after vertically-shifted.